HEATED FRICTION STIR WELDING: AN EXPERIMENTAL AND THEORETICAL INVESTIGATION INTO HOW PREHEATING INFLUENCES ON PROCESS FORCES

Journal:	*Materials and Manufacturing Processes*
Manuscript ID:	LMMP-2009-0286.R1
Manuscript Type:	Original Article
Date Submitted by the Author:	13-Nov-2009
Complete List of Authors:	Sinclair, Paul; Vanderbilt University, Mechanical Engineering Longhurst, William; Vanderbilt University, Mechanical Engineering Cox, Chase; Vanderbilt University, Mechanical Engineering Lammlein, David; Vanderbilt University, Mechanical Engineering Strauss, Alvin; Vanderbilt, Mechanical Engineering Cook, George; Vanderbilt University, Electrical Engineering
Keywords:	friction, stir, welding, heating, aluminum, experiment, weldabilty, thermal, temperature, controller

Changelog:

Reviewer's comments: "It's necessary to work at the layout of the headlines and the references. With regard to the contents the article is accepted."

Title: removed all caps, font to size 16 from 12, bold text
Authors: font to 'small caps' formatting
Added location in italics

Paper: Removed section numbers, changed all section titles to 'small caps' formatting, changed the line spacing around the section titles to 18 pt above and 6 pt below (from 24 and 12, respectively)

References: Located the example references on the Journal Details 'Instruction for Authors' page here: http://www.tandf.co.uk/journals/journal.asp?issn=1042-6914&linktype=44
I changed around each reference to resemble those examples: removed quotations around article titles, removed underlining from Journal names, changed around the date/volume/issue/page information to resemble the examples.

I believe these changes address the items mentioned by the reviewer, and leave alone the body of the paper which was accepted.

Heated Friction Stir Welding: An Experimental and Theoretical Investigation into how Preheating Influences on Process Forces

PAUL C. SINCLAIR, WILLIAM R. LONGHURST, CHASE D. COX, DAVID H. LAMMLEIN, ALVIN M. STRAUSS, GEORGE E. COOK

Vanderbilt University, Nashville, TN

INTRODUCTION

Developed in the early 1990's in the United Kingdom by The Welding Institute (TWI) [1], Friction Stir Welding (FSW) is a solid-state joining process now used worldwide. During a weld a rotating cylindrical tool is driven along the joint line through the material to be welded, heating the material to a plasticized state and literally stirring the workpieces together. Figure 1 shows a typical FSW arrangement. The horizontal shoulder of the tool contacts the surface of the material while the lower pin is driven through it. Friction between these tool surfaces and the work piece along with plastic deformation within the material create localized heating while the rotation and translation create material flow. As the workpiece approaches its melting temperature heat input from the tool drops off, and thus the joint is produced in a solid state.

With the proper parameters, FSW offers less distortion, improved weld quality, and faster welding speeds than traditional fusion welding techniques. Most FSW tools are capable of welding great distances before wearing out, which combined with the absence of needed filler or flux material means there are no consumables. Finally, this new welding scheme generates no fumes or requires any shielding gasses, and because of the lower level of heating it requires less overall energy than any fusion welding. All of these advantages and efficiencies add together to make FSW a very "green" process [2-4].

Due in large part to these many advantages, FSW has grown rapidly in the material joining community. Nearly all imaginable types of joint configurations are now being welded and tools have grown increasingly advanced and more effective as the heating and flow mechanisms are slowly understood [4]. Probably the most important growth has been in the selection of materials being welded. The field started out welding aluminum and its alloys with tools made of steel. There is pressure from the transportation, space, oil and gas industries to FSW higher strength materials, specifically various steel and titanium alloys. While these welds have been conducted successfully, welding these materials generates much higher welding temperatures, resulting in vastly accelerated tool wear [4, 5]. The general response of the FSW community to the problem has been to create tougher tools: going to refractory alloys such as tungsten-carbide (W-C) or ceramics such as polycrystalline cubic boron nitride (PCBN). These tools have produced sound welds in steel and titanium alloys, but drive up the cost and difficulty of the FSW process [6].

The difficulties with higher strength material FSW has prompted a look into how to reduce the forces experienced by the tool. This goal has a number of sought-after benefits: reduced tool wear and clamping forces, allowing faster travel speeds, and even lower energy consumption. One way this is accomplished is with more advanced tool designs, such as the development of the Trivex pin by TWI [7]. Another method with growing popularity is to add

an additional heat source just in front of the FSW tool. This reduces the heat input required from the tool and thus the process loads [5].

A simple method to implement another heat source is to attach some other heating instrument, often some sort of under-powered fusion welding tool, just in front of the FSW tool. This approach is often termed "hybrid-" or "assisted-FSW". Oak Ridge National Lab has added a laser welding system to FSW and reported seeing 50% drops in the welding forces [8]. Several patents have been issued on other laser-assisted FSW processes and improvements [9]. Another patent claims a similar pre-heating system, this time with a TIG arc-welding torch, which reduces FSW tool wear, extends the range of FSW to harder materials, and helps join dissimilar metals [10]. One more assisted-FSW system was constructed by Grant et al. [11] to help weld in cast iron. Even when using W-Re and PCBN tools tool wear had become a major problem. The authors implemented an induction heating system in front of the FSW tool to warm the cast iron with induction heating. The authors reported great reductions in the X and Y tool forces; however, there was no indication of the temperature the heating system achieved or the distribution of that temperature within the work piece.

Probably the most precise heating data in the FSW literature to date comes from Riichi et al. [12]. This group studied the feasibility of FSW pre-heated aluminum by studying the cross sections and the tensile strength of welds in 5052-H34 aluminum after heating to 150, 200, 300, 350, and 400 ^{o}C. The preheating was done by placing a large electric heating element within the backing anvil of the system and insulating the weld from the clamping system. This paper concludes that FSW with heating is indeed feasible, although their 350 and 400 ^{o}C welds showed definite signs of excessive heat input. Perhaps more importantly Riichi et al. showed that there was very little effect on the tensile strength of the welds, showing at most a 15% drop in the tensile strength of the joint in their 150 ^{o}C heated welds. Unfortunately the authors did not measure the FSW processing forces.

The overall goal of the experiments herein described was to describe and analyze the effects of manipulating the initial temperature of the work piece in FSW.

METHODS

The Welding Automation Laboratory at Vanderbilt University uses a modified Milwaukee #2K Universal Milling Machine for FSW. The machine table has been modified to provide computer control along all three axis, which gives greater reliability and precision in the welding process. A Kistler Rotating Cutting Force Dynamometer records welding forces as well as torque. Because the investigation was concerned with FSW process forces and not the actual joint optimization or strength, all welds conducted were bead on plate welds where the tool rotates through a solid work piece. The weld samples were plates of AA 6061-T6 aluminum, nominally 0.250" thick, 3" wide, and 9" long. The FSW tool was made from H-13 tool steel heat treated to RC 48-50. It featured a 0.625" diameter shoulder and a 0.250" side-length Trivex pin ground down to be 0.237" long. Based on previous work the tool was put on a 1^{o} tilt angle and 0.0074" plunge depth to achieve 80% shoulder contact; all this geometry combined to give a joint ligament of just under 0.01"

Samples were heated prior to welding using a ceramic heater placed underneath the aluminum. A small anvil was constructed out of precision-ground AISI 1006 mild steel to sit over the heating element and protect it from the welding forces. A wide strip of G7 Glass-Silicone laminate was placed under the heating element and anvil, and thin strips were placed on top of the aluminum samples to insulate the system from the welding machine and clamps. The

heating system used a basic thermostat controller with a programmed desired temperature. Material temperatures were monitored with two braided J-type thermocouples embedded 0.600" deep in the aluminum samples, one on the advancing side 2" from the start of the sample, and one on the retreating side 2" before the end. The entire system can be seen in Figure 2. While the heating strip controller was simplistic, careful monitoring meant the initial material temperatures were always within ±2 °C of the desired value.

The first matrix of welds consisted of four traverse speeds and eight initial aluminum temperatures. The traverse speeds covered the possible range of values for the Vanderbilt FSW machine. The initial material temperatures were chosen based on the work of Riichi et al. [12]: they reported achieving good welds up to the 300 °C level of material temperature. Because the autozero process was carried out before the heating, the plunge depth was decreased for the higher initial temperature welds to accommodate the effects of thermal expansion: plunge depth was 0.0072" initially, 0.0064" for the 150 and 200 °C welds, and 0.0056" for the 250 and 300 °C welds. The weld matrix and naming convention is shown in Table 1.

A second weld matrix was constructed to investigate preheating effects from another angle: instead of using standard position control welding and recording the forces, a force control process was implemented and the traverse speeds were recorded. The programming and initial research for force control welding was done by graduate student Russell Longhurst [13]. The particular controller model used monitored the axial force of the weld and controlled the traverse speed. The desired axial force was chosen to be 4 kN for all force control welds; the initial traverse speed of each weld was estimated based on the previous work. During the weld a basic proportional controller scheme was used to achieve the desired axial force by adjusting the traverse speed. The characteristic equation for the controller is shown here as equation 1:

$$\text{Delta} = (1.0 / 2000.0) \times \text{FcnGain} \times \text{Error} \quad (1)$$

Delta is the adjustment applied to the traverse speed; Error is the difference between the measured and input axial forces. The proportional gain (FcnGain) was set to two based on previous work done with this force control model and the Trivex tool. This gave an overall proportional gain of 1 ipm change for every 1000 N of error. The force control weld matrix, naming convention, and initial traverse speeds can be seen in Table 2.

RESULTS

For the position control weld matrix, the axial force is of primary interest. Initial graphs of the axial force over the time of the weld showed significant noise, so the data was put through a moderate 9-point moving average filter to make comparisons easier. The average axial force for each weld was found from a 20 second window of the steady-state portion of the weld, as the 14 ipm welds only include about 30 seconds of steady state data. Welding torque was calculated in the same way for each weld. These average axial forces are presented in Figure 3 and clearly show an overall decreasing trend for all four travel speeds, though each shape definitely has a higher-order polynomial curve about it: the axial forces decrease initially, rise after a local minimum, and then falling off again at the highest temperatures. Figure 4 shows normalized values.

The average torque was also computed for each of the position control welds. Since all welds were performed at 2000 rpm, or 33.33 Hz, the power figures are exactly proportional to the torque values. Both average torque and average power for these welds are graphed in Figure 5, and the normalized values presented in Figure 6. Unlike the axial force graphs, the decreasing

trend in the torque graphs seem to be much closer to linear, though at the higher temperatures they appear to begin converging.

Cross-sections for the position control welds were remarkably consistent. A wormhole was found in nearly every weld on the lower advancing side of the nugget. The size of the wormhole varied with the initial temperature of the weld; the procession can be easily seen in Figure 7, which shows the macrographs of all eight 11 ipm welds. The hole in the bottom of weld H11 was created when removing the weld from the anvil, as the welding forces had partially joined the aluminum to the steel. In about half the welds there was a surface lack of fill defect, seen on the top of the weld also on the advancing side: in Figure 7, welds B11, C11, and D11 all show this. In some welds it is observed that the two defects seem to be related – the worm hole defect travels up to the surface hole – indicating a lack of flow along the entire AS of the weld nugget. This is seen in weld C14, shown in Figure 8.

The results for the force control weld matrix show that the basic proportional controller model is working very well. Figure 9 shows a typical force control data plot. In the last half of each weld, as a steady state welding process was reached, the errors in the axial force were generally less than ±100 N.

The average speed values were computed from the last half of each weld. These average values, plotted against the controlled initial aluminum temperature, are given in Figure 10.

DISCUSSION

Overall the heating of the aluminum with an additional source beyond the FSW tool has definitely reduced the major process force associated with this new type of welding. As shown in Figure 4, with even small amounts of heating, the average axial force of welding AA6061 at some temperature dropped by a minimum of 21% for all welding traverse speeds. The maximum reduction seen was a great 43% reduction in force for weld F05 compared to the A05 control weld. These magnitudes are in agreement with the limited data found in literature [8]. Thinking another way, by adding even slight preheating capabilities the travel speed or tool life of FSW can be significantly improved. If a tool was shown to have good wear characteristics under a certain load, the allowable travel speed could be easily doubled or almost tripled with additional energy input. The force-control welds support this last point in the strongest possible way. Given a constant force input, Figure 10 demonstrates how much faster the system can travel for a given initial material temperature. The final data point on the graph should be a bit higher in fact – that is, traversing faster – but the force controller equation hit upon the 14 ipm machine limit.

Certainly the most intriguing result from the position control welds is the definite trend exhibited by all four traverse speed weld series in Figure 3. In each group, as the initial aluminum temperature increases, the average axial force decreases. This behavior was expected given aluminum's yield strength dependence on temperature, as shown in Figure 11. Between 100^{o} and 250^{o} C pre-heating, however, each traverse speed trend actually increases, passing through an inflection point at around 150^{o} C. After reaching a local maximum axial force at 200 or 250^{o} C, each trend line finally drops off again at the highest temperatures. The characteristics of the trend definitely seem to be influenced by the travel speed. As the travel speed increases, the location of the local minimum moves to lower temperatures, and the latter half of the curves are broader than welds performed at slower traverse speeds.

The large worm holes present in nearly all of the welds, along with the surface lack of fill defects, are a somewhat expected result given the use of the Trivex welding tool. While the tool design does provide more stirring action than a basic cylindrical pin it still lacks any of the

surface features well known for creating lots of material flow. Kumar and Kailas discuss the presence of two primary flows in FSW: the first is a vertical pin-driven flow and the second a rotational shoulder-driven movement [15]. The worm holes in the bottom corner of the nugget suggest that the pin is not transporting enough material vertically. Further, the shoulder is letting material escape the tool before it can bring it around behind the pin. It is clear the defects in this particular experiment would be effectively reduced or eliminated with the use of a different tool design. A simple inclusion of threads – a common FSW tool feature – would create a vastly improved pin flow.

MODELING OF HEATED FSW

To help explore the process forces and flows of heated FSW, the finite volume Computational Fluid Dynamics (CFD) solver Ansys FLUENT was used with implicit formulation to create a model of the welding process. The model was constructed by Vanderbilt graduate students David Lammlein and Chase Cox. The weld material viscosity function was set to Carreau model viscosity with a time constant $\lambda = 10$ seconds, power-law index n=0.2, reference temperature α=300, zero-shear viscosity 1e8 kg/m/s, and infinite shear viscosity of 0.001003 kg/m/s. The total heat input was calculated via the weld power method [16-24]:

$$P = \omega \cdot M \quad (2)$$

$$Q = P \cdot \eta_{thermal} \cdot \eta_{conduction} \quad (3)$$

where P is the weld power (W), Q is the heat input to the tool and weld material (W), ω is the tool rotational speed (rad/s), M is the measured torque (N·m), $\eta_{thermal}$ is the fraction of mechanical work dissipated as heat into the tool shank and the weld, and $\eta_{thermal}$ is the fraction of that heat input into the weld. Values of 0.90 and 0.75 are used respectively for these terms and are found to be reasonable for the conditions of the current study. The measured torque values came from the 5 ipm weld series in Figure 5. This calculated total tool heat input was then applied in the model at the tool-material interface via a user-defined function which varies heat input over the tool surface according to the local tangential velocity magnitude. Heat input is therefore highest near the tool shoulder edge and zero at the center of the probe tip with the total tool heat input equal to the weld power. A variable slip-shear condition was set at the weld interface. The tool rotational velocity was set to 72% of the experimental parameter and a pure stick condition was used. This simple boundary condition was used because the actual relationship is unknown and unwarranted complexity is not desired in the model.

The CFD model consists of 171,395 tetrahedral elements which accurately reflect the experimental geometry. The tool traverse was imposed in the model by leaving the tool at the model origin and establishing a velocity inlet and pressure outlet for the aluminum plate. Element refinement was increased towards the weld interface; the surface elements of the tool pin are seen in Figure 12. The thermal boundary conditions used in the model are show in Figure 13.

Interestingly, the same general trend seen in the average axial force data for the position control welds is seen to a small extent in the force data from the CFD model, seen in Figure 14. This definitely helps confirm a few things about the experimental results. The FLUENT results suggest that the axial force curves are do the process of FSW with a Trivex tool in AA 6061-T6,

and not artifacts created by the elaborate insulated, raised-anvil setup built to heat the welds in the first place.

The FLUENT results also help to understand the mechanism behind the fluctuating average force values. One plausible explanation was that the heating period before the weld began was acting to heat treat the aluminum weld samples. Even with the fast powerful mica heating element, the higher initial temperature welds took some minutes to reach those initial temperature – as long as 15 minutes for the hottest welds – and it was speculated that the time allowed some type of precipitation hardening to begin, strengthening the aluminum above expected values. However, the CFD model does not contain this heating time and yet exhibits the same basic force trend; we must conclude that the axial force fluctuation over initial temperature comes from material properties and FSW mechanics themselves.

CONCLUSIONS

While "preheating" or "assisted" FSW has been suggested and performed by many, this is one of the first studies to take a measured and controlled look at how that heating affects the process forces of this relatively new joining technique. Already here at Vanderbilt another graduate student is using the heating set-up to help his attempts to reduce forces and increase stirring while joining dissimilar materials. As seems usual in FSW, the experimental work into preheating has outpaced the technical understanding of the process. Hopefully this experiment, while still an experimental approach, can help prompt more controlled examinations and a better understanding of the preheating process.

REFERENCES

1. Thomas, W. M., Nicholas, E. D., Needham, J. C., Murch, M. G., Templesmith, P., and Dawes, C. J. G.B. Patent Application No. 9125978.8 December 1991.
2. Ma, Z.Y. Friction Stir Processing Technology: A Review. Metallurgical and Materials Transactions A **2001**, 39 (3), 642-658.
3. Balasubramanian, V. Relationship between base metal properties and friction stir welding process parameters. Materials Science and Engineering A **2008**, 480 (1-2), 397-403.
4. Mishra, R. S., and Ma, Z. Y. Friction stir welding and processing. Materials Science and Engineering: Research Reports **2005**, 50, 1-78.
5. Nandan, R., DebRoy, T., and Bhadeshia, H.K.D.H. "Recent Advanced in Friction Stir Welding – Process, Weldment Structure and Properties." Progress in Materials Science Vol. 53, No. 6 (2008): 980-1023.
6. Bernath, Jeff. Personal Communication. 7 November 2008. <jbernath@ewi.org>.
7. Colegrove, P. A., and Shercliff, H. R. Development of Trivex friction stir welding tool (Parts 1 and 2). Science and Technology of Welding and Joining **2004**, 9 (4), 345-361.
8. Cabage, Bill. New way to weld. Oak Ridge National Laboratory Reporter **2006**, 84.
9. Palm, Frank. Laser supported friction stir welding method. United States Patent 6,793,118. September 2004.
10. Kou, S., and Cao, G. Arc-enhanced friction stir welding. United States Patent 7,078,647. July 2006.
11. Grant, G. J., Khaleel, M., Eberhardt, J. J., Arbegast, B., Stone, G., Howard, S., and Allen, C. Friction stir joining and processing of advanced materials including MMCs. High Strength Weight Reduction Materials **2005**, 112-121
12. Suzuki Riichi, Takahashi Takehiko, Hioki Susumu, Yamamoto Naoki, and Kaneko Yuuta. On pre-heating effect for friction stir welding of aluminum alloy – A feasibility study of friction stir welding with heating of aluminum alloy (Report 1). Quarterly Journal of the Japan Welding Society **2006**, 24 (3), 281-286
13. Longhurst, William R., Strauss, Alvin M., Cook, George E. Enabling of Robotic Friction Stir Welding: The Control of Weld Seam Heat Distribution by Traverse Speed Force Control. Manuscript submitted for publication.
14. Crawford, Reginald. A Mechanistic Study of the Friction Stir Welding Process. Dissertation, Vanderbilt University. August 2006.
15. Kumar, K., and Kailas, S. V. The role of friction stir welding tool on material flow and weld formation. Materials Science and Engineering A **2008**, 485, 367-374.
16. Sellars, C.M., and Tegart, W.J.M. Hot Workability. International Metallurgical Reviews **1972**, 17, 1-24
17. Nandan, R., Roy, G. G., and Debroy, T. Numerical Simulation of Three-Dimensional Heat Transfer and Plastic Flow During Friction Stir Welding, Metallurgical and Materials Transactions **2006**, 37A, 1247-1259
18. Simar A., Pardoen T., and de Meester B. Influence of friction stir welding parameters on the power input and temperature distribution on friction stir welding, Proc. of the 5th International Symposium on Friction Stir Welding, Metz, France, Sept. 14-16, 2004.

19. Simar A., Pardoen T., and de Meester B. Effect of rotational material flow on temperature distribution in friction stir welds. Science and Technology of Welding and Joining **2007**, 12 (4), 324.
20. Santiago D.H., Lombera G., and Santiago U. Numerical modeling of welded joints by the friction stir welding process. Materials Research **2007**, 7 (4), 569.
21. Pew J.W., Nelson T.W., and Sorensen C.D. Torque based weld power model for friction stir welding. Science and Technology of Welding and Joining **2007**, 12 (4), 341.
22. Russell M.J., and Shercliff H.R. Analytical modeling of microstructure development in friction stir welding, Proc. of the 1st International Symposium on Friction Stir Welding, session 8, Thousand Oaks, California, June 14-16, 1999.
23. Milding O.T., and Grong O. A process model for friction welding of Al-Mg-Si alloys and Al-SiC metal matrix composites. Acta Metall. Mater **1994**, 42 (5), 1595.
24. Frigaard O., Grong O., Bjorneklett B., and Midling O.T. Modelling of thermal and microstructure fields during friction stir welding of aluminium alloys, Proc. of the 1st International Symposium on Friction Stir Welding, session 8, Thousand Oaks, California, June 14-16, 1999.

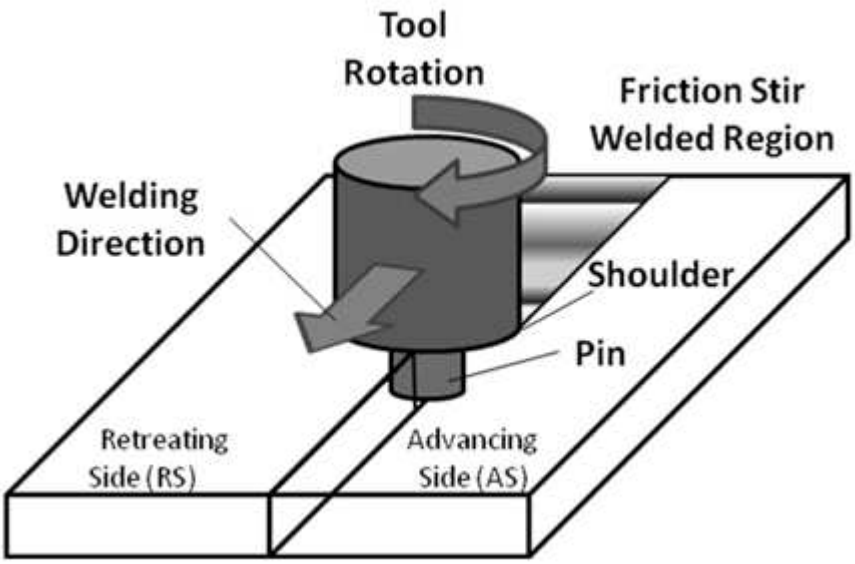

Figure 1. Schematic of Typical FSW Process
162x105mm (72 x 72 DPI)

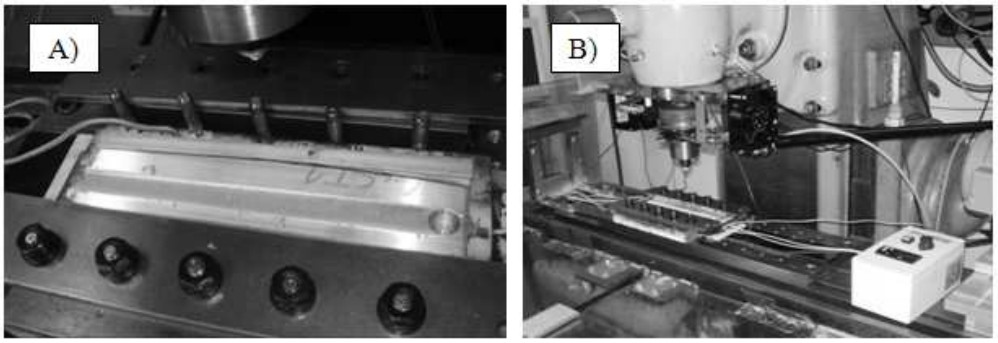

Figure 2. Heated FSW System (A) A picture of the anvil and clamping setup with one clamp removed. One of the J-type braided thermocouples can be seen in the aluminum. (B) The entire welding setup.

217x74mm (72 x 72 DPI)

Traverse Speed (ipm)	Initial Welding Temperature (°C)							
	22	50	75	100	150	200	250	300
5	A05	B05	C05	D05	E05	F05	G05	H05
8	A08	B08	C08	D08	E08	F08	G08	H08
11	A11	B11	C11	D11	E11	F11	G11	H11
14	A14	B14	C14	D14	E14	F14	G14	H14

Table 1. Position Control Weld Matrix. No shading indicates 0.0072" plunge depth, vertical shading is 0.0064", and horizontal is 0.0056"
170x64mm (72 x 72 DPI)

Initial Welding Temperature (°C)	Weld Name	Initial Traverse Speed (ipm)
22	Act	5
50	Bct	5
75	Cct	5.5
100	Dct	5.5
150	Ect	7
200	Fct	7
250	Gct	8
300	Hct	8

Table 2. Force Control Weld Matrix
115x70mm (72 x 72 DPI)

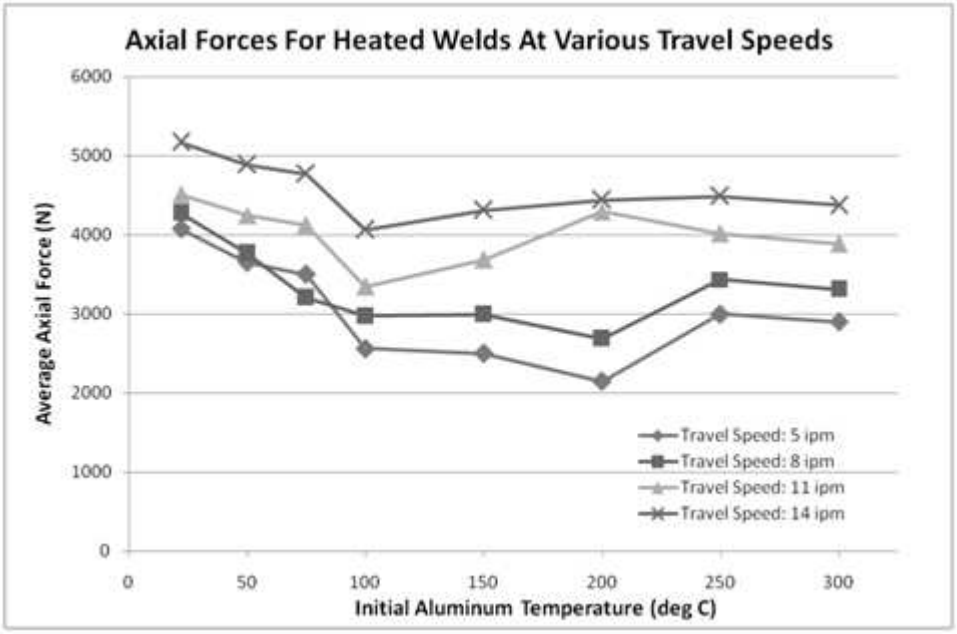

Figure 3. Average Axial Forces for the Position Control Welds
170x111mm (72 x 72 DPI)

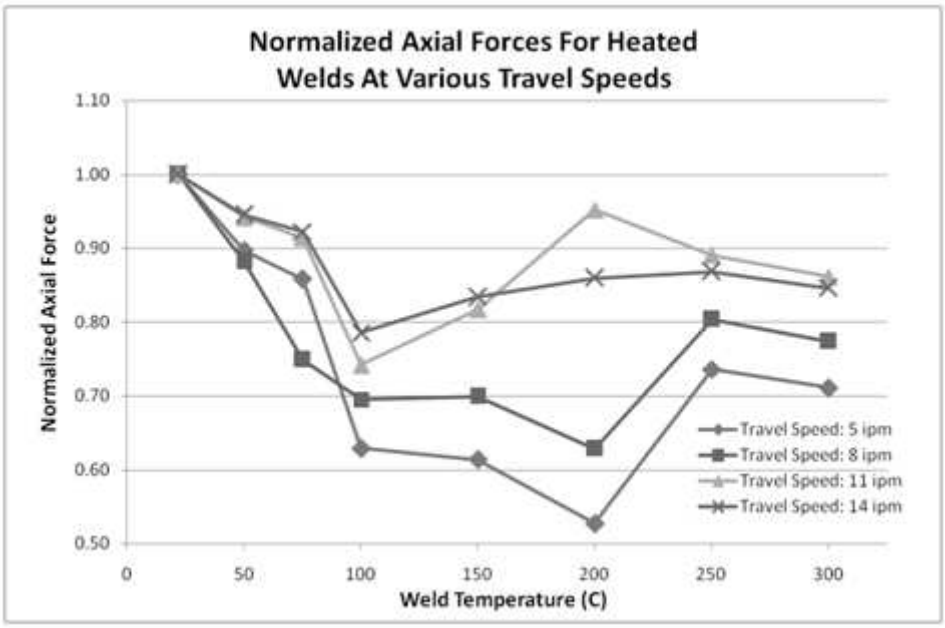

Figure 4. Normalized Axial Forces for the Position Control Welds
168x111mm (72 x 72 DPI)

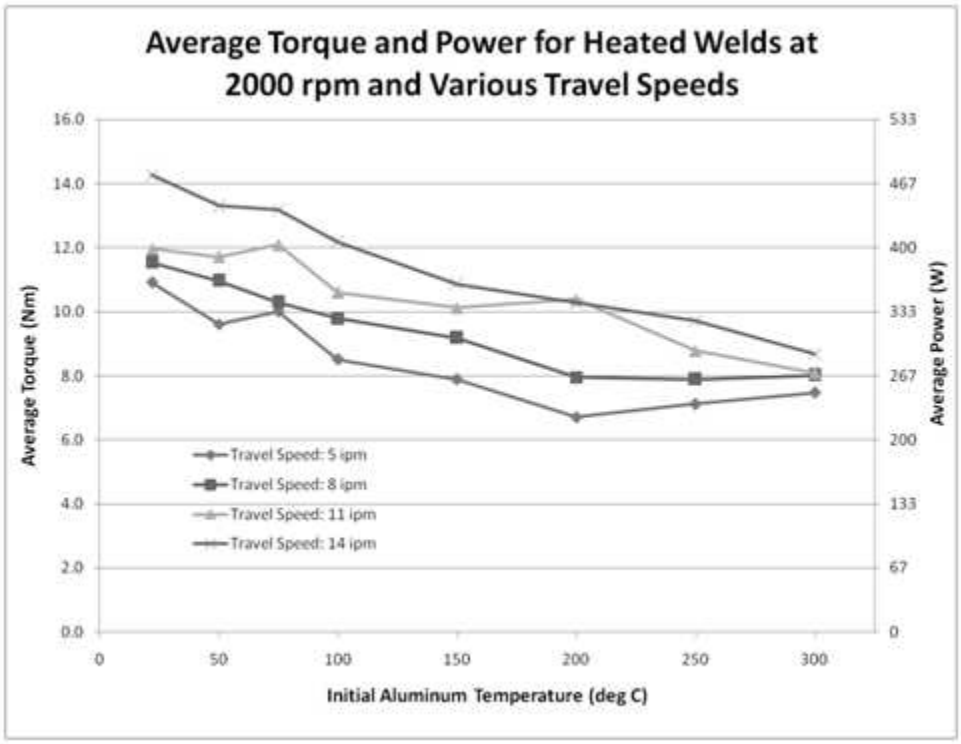

Figure 5. Average Torque and Power Values for the Position Control Welds
172x133mm (72 x 72 DPI)

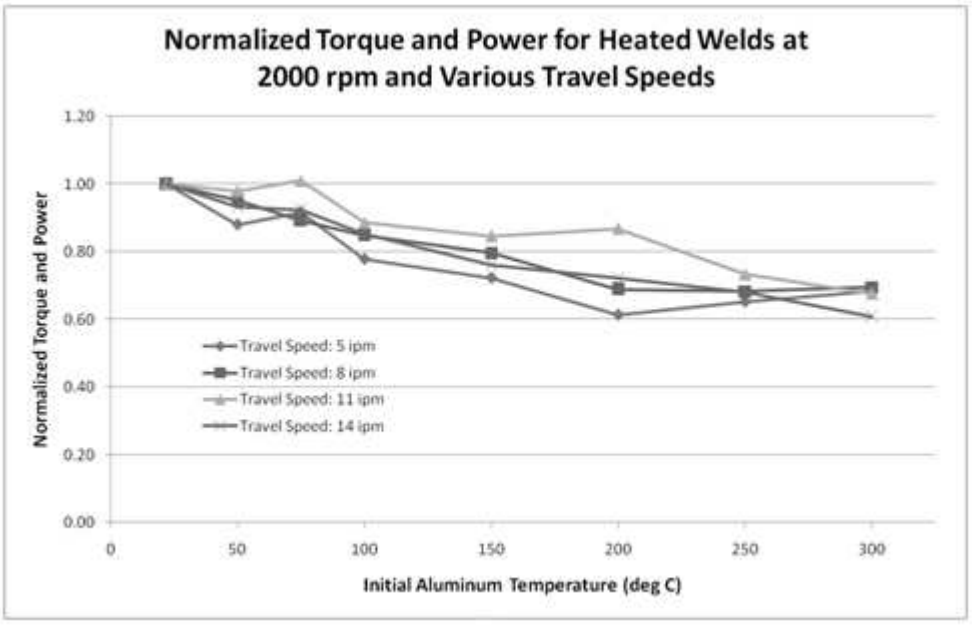

Figure 6. Normalized Axial Forces for Heated Welds at Various Travel Speeds
173x111mm (72 x 72 DPI)

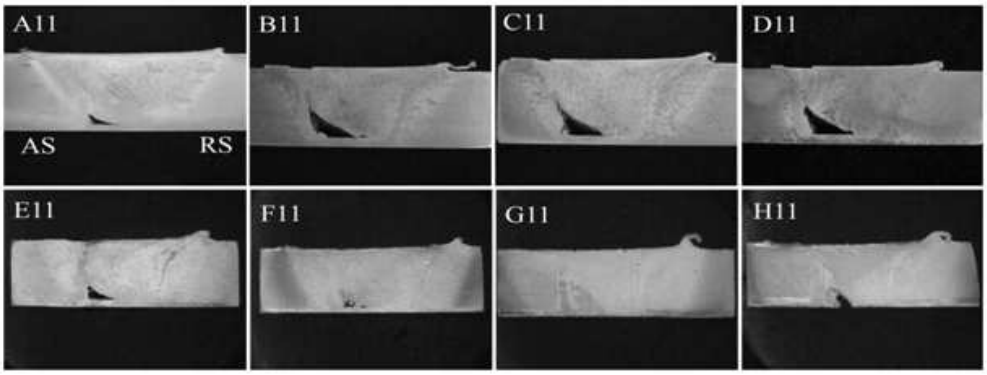

Figure 7. Macrosections of the 11 ipm Welds
217x83mm (72 x 72 DPI)

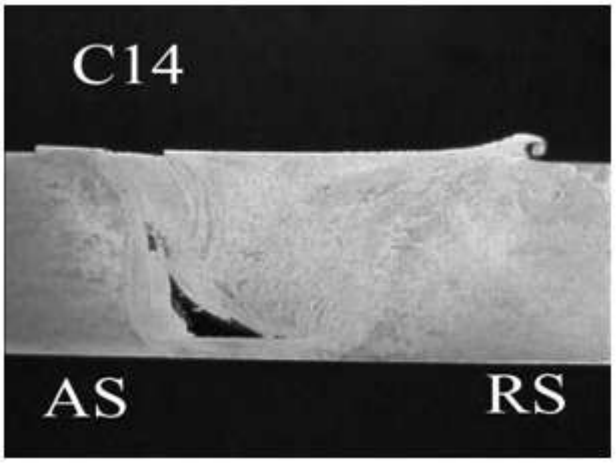

Figure 8. The Connection Between the Two Defects
112x82mm (72 x 72 DPI)

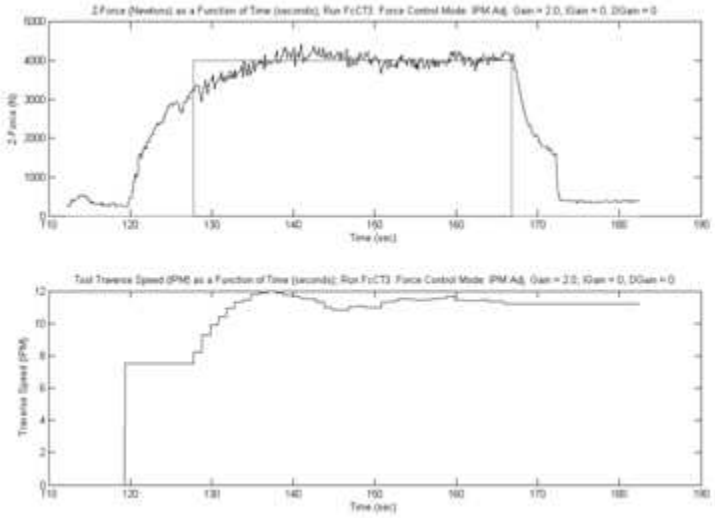

Figure 9. Example Force Control Weld Data: Weld Fct
134x94mm (72 x 72 DPI)

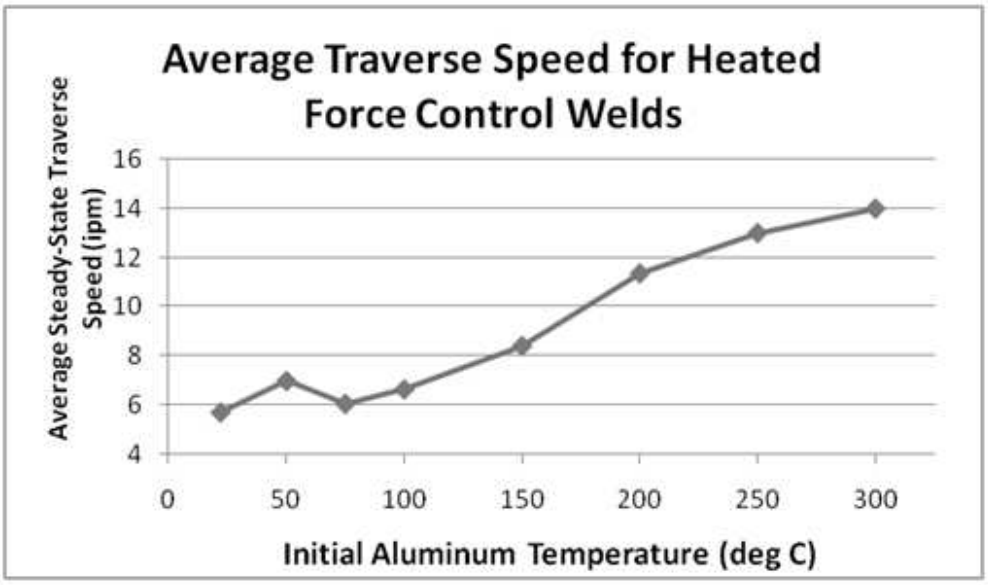

Figure 10. Average Force Control Weld Results
181x107mm (72 x 72 DPI)

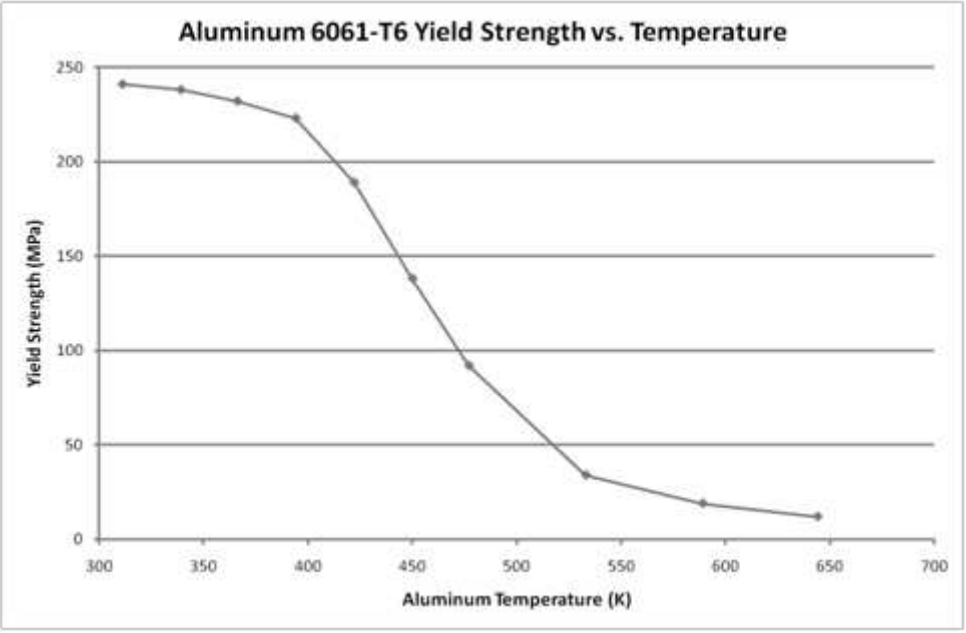

Figure 11. Aluminum 6061-T6 Yield Strength Dependence on Temperature [14]
174x114mm (72 x 72 DPI)

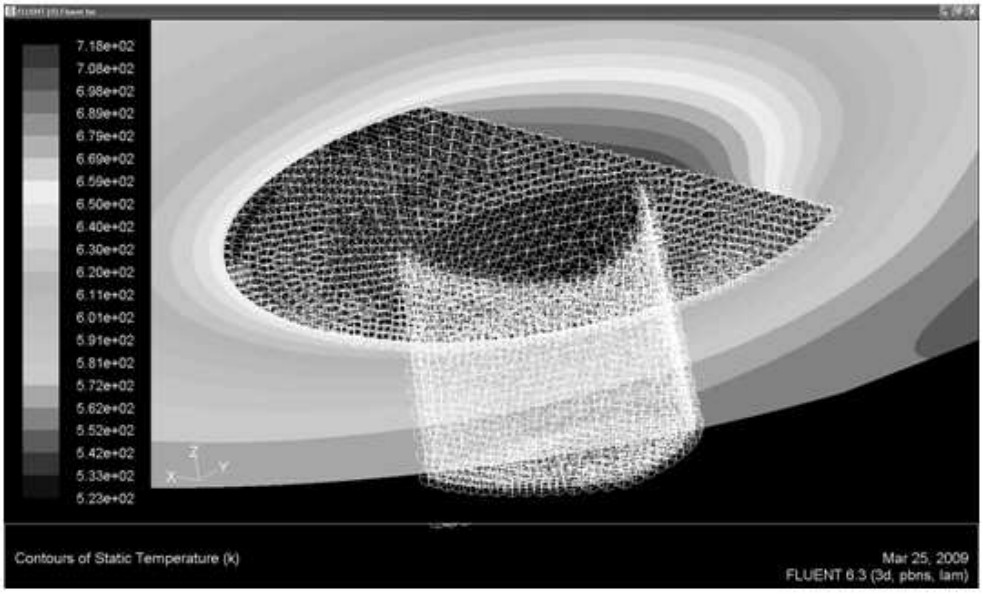

Figure 12. Detail of the Trivex Pin Model Elements
194x116mm (72 x 72 DPI)

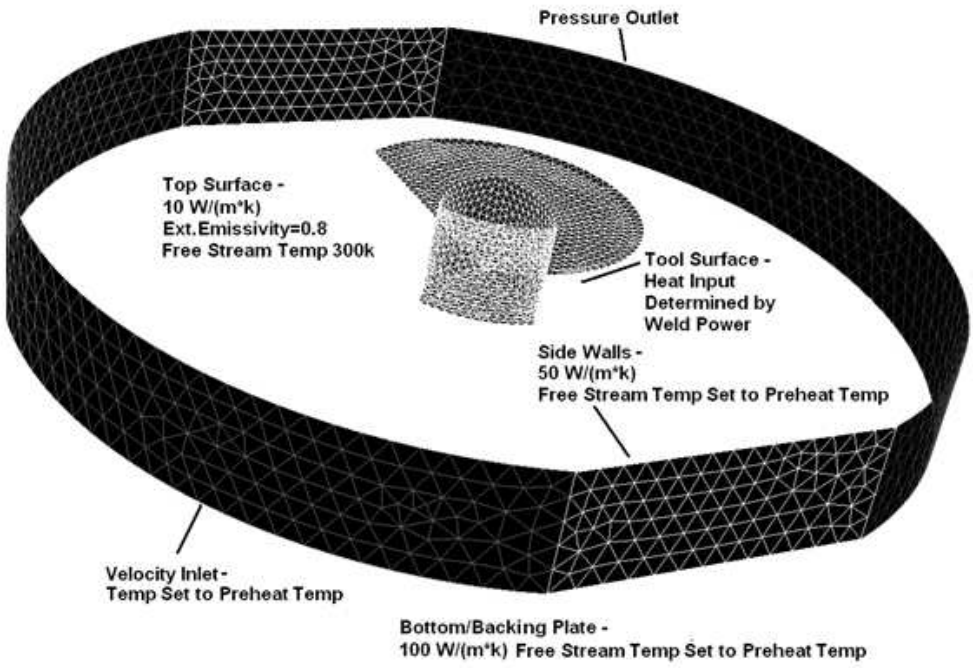

Figure 13. FLUENT Model Thermal Boundary Conditions
202x137mm (72 x 72 DPI)

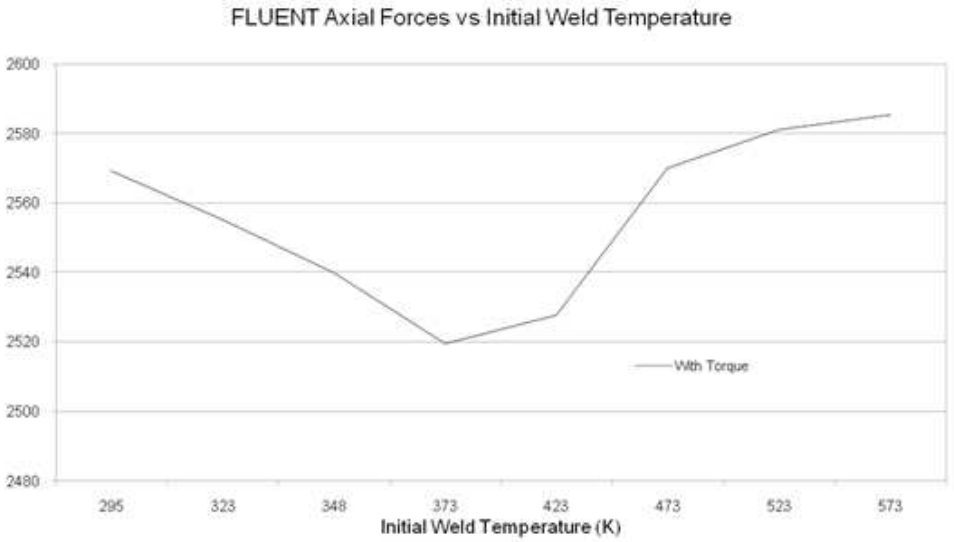

Figure 14. FLUENT's Axial Forces for Varying Initial Weld Temperatures
195x110mm (72 x 72 DPI)